

Early-Warning Signals of Grokking via Loss-Landscape Geometry

Yongzhong Xu*

Abstract

Grokking refers to the phenomenon in which neural networks abruptly transition from memorization to generalization after extended training. Recent work on modular arithmetic has linked grokking to prolonged confinement on low-dimensional execution manifolds in weight space, followed by a sudden escape into a generalizing solution. A central open question is whether this geometric mechanism extends beyond arithmetic tasks.

We investigate this question on two structurally distinct sequence-learning problems: the SCAN compositional generalization benchmark and Dyck-1 language depth prediction. Across both tasks and a wide range of learning rates, we find that the commutator defect—a measure of loss-landscape curvature derived from the non-commutativity of successive gradient updates—reliably rises well before the onset of generalization. The lead time between defect onset and grokking follows a power-law relationship with the grokking timescale, with exponents $\alpha \approx 1.18$ for SCAN ($R^2 = 0.990$, $n = 11$) and $\alpha \approx 1.13$ for Dyck ($R^2 = 0.908$, $n = 14$). Combined with prior results on modular arithmetic, all three task families exhibit superlinear scaling ($\alpha > 1$), yielding advance warning windows of 90–97% at slow learning rates.

Weight-space principal component analysis reveals task-dependent spectral dynamics: PC1 de-concentration precedes grokking in Dyck and modular arithmetic but follows it in SCAN, indicating that spectral concentration is not a universal precursor. In contrast, the commutator defect consistently anticipates generalization across all settings. A three-basis integrability decomposition shows that defect spikes reflect structured non-commutativity within the learning subspace, characteristic of the grokking regime.

Finally, causal interventions on both SCAN and Dyck demonstrate a mechanistic role for the defect: perturbations that amplify non-commutativity accelerate grokking (by $\sim 32\%$ on SCAN and $\sim 50\%$ on Dyck), whereas suppressing orthogonal gradient flow delays or prevents generalization. The three task families form a spectrum of causal sensitivity: modular arithmetic is rigid (boosting has no effect), Dyck is responsive (both mild and aggressive boosting accelerate), and SCAN is intermediate (mild boosting accelerates but aggressive boosting destabilizes). Across all tasks, suppression delays or prevents grokking, establishing necessity as a universal finding. Together with prior results, our findings establish the commutator defect as a robust, architecture-agnostic, and causally implicated early-warning signal for grokking in transformer-based models.

1 Introduction

Grokking—the phenomenon where neural networks trained on small datasets first memorize the training set and then, long after achieving perfect training accuracy, suddenly generalize to the test set—was first reported by Power et al. [2022] in modular arithmetic tasks. The phenomenon challenges conventional accounts of generalization because standard training metrics (loss, accuracy)

*abbyxu@gmail.com

provide no advance warning: a model with perfect training accuracy and poor test accuracy might be on the verge of grokking, or might never generalize at all.

In our prior work [Xu, 2026b], we proposed a geometric account of grokking centered on *transverse curvature dynamics*. Working on modular arithmetic (six binary operations mod 97), we showed that:

1. Weight-space trajectories during grokking lie on a rank-1 *execution manifold* (PC1 captures 68–83% of variance);
2. This manifold exhibits empirical invariance: commutator defect vectors—measuring the non-commutativity of successive gradient updates—are predominantly orthogonal to it ($\rho \approx 1.000$);
3. Curvature explodes in the normal bundle (10–1000 \times), with onset preceding generalization by 600–1600 steps;
4. The lead time obeys a power law $\Delta t \propto t_{\text{grok}}^\alpha$ with $\alpha = 1.27 \pm 0.03$ ($R^2 = 0.97$, $n = 43$) across a 300 \times learning-rate sweep;
5. Causal interventions confirm that orthogonal gradient flow is necessary (suppression prevents grokking) but curvature boosting alone is not sufficient (no acceleration).

A fundamental open question raised by that work is whether these findings are specific to modular arithmetic and encoder-only transformers, or whether they reflect a universal geometric mechanism of grokking. The original paper noted that “preliminary experiments on Dyck languages and the SCAN compositional-generalization benchmark suggest that qualitatively similar low-dimensional confinement and transverse curvature dynamics arise beyond modular arithmetic; a systematic investigation of these settings is ongoing.”

This paper provides that systematic investigation. We extend the commutator defect analysis to two structurally distinct tasks:

1. **SCAN** [Lake and Baroni, 2018]: A compositional generalization benchmark mapping natural language commands (e.g., “jump twice”) to action sequences (e.g., JUMP JUMP), trained with an encoder–decoder transformer.
2. **Dyck-1 depth prediction**: A formal language task where a causal (decoder-only) transformer must predict the current stack depth at each position in a parenthesis sequence, trained on only 50 examples.

These tasks differ from modular arithmetic in architecture (encoder–decoder and causal vs. encoder-only), input domain (natural language and formal language vs. numerical), output type (sequence generation and per-token classification vs. single-token classification), and dataset structure.

Key contributions. Our work makes six main contributions:

1. **Universality of defect onset.** On both SCAN and Dyck, the commutator defect onset reliably precedes the generalization transition across all tested learning rates—15 of 15 grokking runs on Dyck and 11 of 11 on SCAN show positive lead time.
2. **Super-linear scaling.** The lead time obeys a power law with super-linear exponent on both tasks: $\alpha \approx 1.18$ ($R^2 = 0.990$) for SCAN and $\alpha \approx 1.13$ ($R^2 = 0.908$) for Dyck. Combined with modular arithmetic ($\alpha \approx 1.3$), all three task families exhibit $\alpha > 1$.

3. **PC1 dissociation.** Weight-space PC1 de-concentration precedes grokking on Dyck (as in modular arithmetic) but *follows* grokking on SCAN, demonstrating that the commutator defect is a more universal signal than spectral concentration.
4. **Integrability decomposition.** A three-basis analysis (Weight SVD, ΔW SVD, Gradient SVD) shows that the defect spike reflects structured non-commutativity aligned with the learning subspace (exec/random ratio 2–3×), specific to the grokking regime.
5. **Causal evidence.** On both SCAN and Dyck, perturbations that amplify the commutator accelerate grokking ($\sim 32\%$ on SCAN, $\sim 50\%$ on Dyck); perturbations that suppress orthogonal gradient flow delay or prevent it. The three task families (including modular arithmetic) form a spectrum of causal sensitivity, while universally confirming necessity.
6. **Instability regime.** At high learning rates (Dyck, $\eta = 10^{-2}$), accuracy oscillates rather than transitioning cleanly, motivating sustained-accuracy grokking criteria.

Paper outline. Section 2 reviews the geometric framework of Xu [2026b]. Section 3 describes the experimental setup. Section 4 presents the methods: PCA eigenanalysis, commutator defect measurement, and integrability decomposition. Section 5 presents results in four stages: SCAN (Section 5.1), Dyck (Section 5.2), geometric analysis (Section 5.3), and causal interventions (Section 5.4). Section 6 synthesizes the cross-dataset comparison. Section 8 discusses implications and connections to broader themes.

2 Background: Geometric Framework for Grokking

We review the geometric framework introduced in our prior work [Xu, 2026b] for studying grokking through the lens of loss-landscape curvature. This section defines the key mathematical objects and establishes the theoretical context for the present work.

2.1 Grokking

Power et al. [2022] first reported grokking on modular arithmetic tasks, showing that small transformers can memorize training data in hundreds of steps but require thousands to generalize. Subsequent work has shown grokking in diverse settings including group operations [Nanda et al., 2023], boolean functions, sparse parities [Barak et al., 2022], and compositional generalization [Murty et al., 2023]. The phenomenon is sensitive to regularization strength [Liu et al., 2022], dataset size [Liu et al., 2023], and learning rate.

2.2 The Execution Manifold

Following our earlier work [Xu, 2026b], we define the *execution manifold* as the low-dimensional subspace of parameter space traced by the weight trajectory during training. Formally, given T weight snapshots $\{W_t\}_{t=1}^T$ of a weight matrix $W \in \mathbb{R}^{d \times d}$, we form the trajectory matrix of displacements from initialization:

$$X = \begin{pmatrix} \text{vec}(W_1 - W_0) \\ \vdots \\ \text{vec}(W_T - W_0) \end{pmatrix} \in \mathbb{R}^{T \times d^2}, \quad (1)$$

after column-centering. The SVD $X = U\Sigma V^\top$ yields principal directions $\{v_k\}$. The explained variance ratio of the k -th component is $\sigma_k^2 / \sum_i \sigma_i^2$, and $\text{PC1\%} = 100 \times \sigma_1^2 / \sum_i \sigma_i^2$ measures the fraction of trajectory variance captured by a single direction.

Definition 1 (Execution manifold). *Let $V_K = [v_1, \dots, v_K]$ denote the top- K right singular vectors of X . The execution manifold is the affine subspace $\mathcal{M} = \{W_0 + V_K \alpha : \alpha \in \mathbb{R}^K\}$ through the initial weights W_0 . When PC1\% is high (> 70%), \mathcal{M} is effectively rank-1: the weight trajectory is confined to a one-dimensional curve in parameter space.*

In modular arithmetic, we found $\text{PC1\%} = 68\text{--}83\%$ across all grokking conditions [Xu, 2026b], with z-scores $5\text{--}20\sigma$ above a random-walk null model.

2.3 The Commutator Defect

The commutator defect quantifies the non-commutativity of gradient updates from different mini-batches, providing a local probe of loss-landscape curvature that requires no Hessian computation.

Definition 2 (Commutator defect). *Given parameters θ_0 , loss function \mathcal{L} , step size η , and two independent mini-batches A, B , define:*

$$\theta_{AB} = \theta_0 - \eta g_A(\theta_0) - \eta g_B(\theta_0 - \eta g_A(\theta_0)), \quad (2)$$

$$\theta_{BA} = \theta_0 - \eta g_B(\theta_0) - \eta g_A(\theta_0 - \eta g_B(\theta_0)), \quad (3)$$

where $g_A(\theta) = \nabla_\theta \mathcal{L}_A(\theta)$ is the gradient on mini-batch A at parameters θ . The scale-normalized commutator defect is:

$$\mathcal{D}(\theta_0; A, B) = \frac{\|\theta_{AB} - \theta_{BA}\|}{\|\eta g_A\| \cdot \|\eta g_B\|}. \quad (4)$$

Geometric interpretation. To first order in η , the commutator vector $\delta = \theta_{AB} - \theta_{BA}$ satisfies:

$$\delta \approx \eta^2 (\nabla g_B \cdot g_A - \nabla g_A \cdot g_B), \quad (5)$$

which is the Lie bracket of the gradient vector fields [Xu, 2026b]. \mathcal{D} is thus proportional to the Lie bracket of stochastic gradient vector fields and serves as a proxy for local nonlinearity of the loss landscape: if the landscape is locally flat (integrable), gradient steps commute and $\mathcal{D} = 0$. A large defect signals that the order of gradient updates matters—the loss landscape has developed curvature structure that breaks path-independence.

2.4 Manifold Projection and Invariance

To determine whether curvature lives inside or outside the execution manifold, we decompose the commutator vector δ relative to the PCA basis [Xu, 2026b].

Definition 3 (Invariance measure). *Let $B \in \mathbb{R}^{P \times K}$ be an orthonormal basis for the PCA subspace embedded in the full parameter space (P total parameters). Given commutator vector $\delta = \theta_{AB} - \theta_{BA}$, decompose:*

$$\delta = \underbrace{BB^\top \delta}_{\delta_{\parallel} \text{ (projected)}} + \underbrace{(\delta - BB^\top \delta)}_{\delta_{\perp} \text{ (residual)}}. \quad (6)$$

The invariance measure is the residual fraction:

$$\rho = \frac{\|\delta_{\perp}\|}{\|\delta\|}. \quad (7)$$

If $\rho \approx 1$, the commutator is orthogonal to the execution manifold—curvature is confined to the *normal bundle*—and the manifold exhibits *empirical invariance* under the optimization dynamics. If $\rho \approx 0$, curvature lies within the learned subspace.

Definition 4 (Transverse decoupling). *The optimization dynamics are transversely decoupled on the execution manifold \mathcal{M} if commutator defect vectors are confined to its normal bundle ($\rho \approx 1$). In this regime, curvature-induced perturbations act almost entirely orthogonally to \mathcal{M} , so that the observed trajectory remains confined to the learned subspace over training.*

In modular arithmetic, we found $\rho \approx 1.000$ within numerical precision across all 36 conditions [Xu, 2026b] (6 operations \times 2 weight-decay settings \times 3 seeds), with the exec/random projection ratio at $1.8\text{--}2.9\times$, confirming that the near-zero parallel component is geometrically structured rather than a dimensionality artifact.

2.5 Random Subspace Control

Because any K -dimensional subspace of \mathbb{R}^P captures $\sim \sqrt{K/P}$ of a random vector, near-unity ρ alone does not confirm geometric structure. Following Xu [2026b], we compare the PCA-basis projection against random baselines: for each commutator vector δ , we compute the projection fraction onto $N_{\text{rand}} = 5$ random K -dimensional orthonormal bases and report the *exec/random ratio* $\text{proj}_{\text{exec}}/\text{proj}_{\text{rand}}$. Values significantly above 1.0 confirm that the PCA subspace captures more commutator energy than expected by chance.

2.6 Scaling Law

We established [Xu, 2026b] that the lead time between defect onset and grokking obeys a power law:

$$\Delta t = C \cdot t_{\text{grok}}^\alpha, \quad (8)$$

where $\Delta t = t_{\text{grok}} - t_{\text{onset}}$ is the lead time, t_{grok} is the grokking step, and t_{onset} is the defect onset step. The *lead fraction* $\Delta t/t_{\text{grok}}$ expresses lead time as a proportion of total training time. In modular arithmetic, $\alpha = 1.27 \pm 0.03$ ($R^2 = 0.97$, $n = 43$) across a $300\times$ learning-rate sweep: because $\alpha > 1$, the predictive window grows super-linearly with grokking timescale.

3 Experimental Setup

3.1 Tasks and Datasets

SCAN Compositional Generalization. We use the SCAN simple split [Lake and Baroni, 2018], randomly sampling $N_{\text{train}} = 2,048$ command–action pairs from the full dataset of approximately 14,000 examples. The remaining examples form the test set ($\sim 9,000$). The command vocabulary contains 21 tokens and the action vocabulary 7 tokens. Maximum command length is 8 tokens and maximum action length is 13 tokens (both plus boundary tokens). The data split is fixed across all runs (data seed = 0).

Dyck-1 Depth Prediction. We generate Dyck-1 sequences of length 24 (maximum nesting depth 12) with a fixed random seed. The model must predict the current stack depth at each parenthesis position: a 13-class classification problem (depths 0–12). The vocabulary contains 3 tokens: open parenthesis, close parenthesis, and padding. We use an extreme data-scarcity regime: $N_{\text{train}} = 50$ sequences, $N_{\text{test}} = 5,000$ sequences. This large train–test ratio amplifies the grokking effect.

Table 1: Architecture comparison across three task families. The Dyck and modular arithmetic architectures share the same encoder structure; SCAN uses a full encoder–decoder.

	Modular Arithmetic	Dyck	SCAN
Architecture	Encoder-only	Causal decoder	Enc–Dec
d_{model}	128	128	256
Layers	2	2	3+3
Heads	4	4	4
d_{ff}	256	256	512
Parameters	~290k	~150k	~1.5M
Output	97-class	13-class/token	Seq. generation
N_{train}	4,704	50	2,048

3.2 Model Architectures

SCAN. We use a standard encoder–decoder transformer with $d_{\text{model}} = 256$, $n_{\text{layers}} = 3$ (each for encoder and decoder), $n_{\text{heads}} = 4$, $d_{\text{ff}} = 512$, and no dropout. The decoder uses causal masking and cross-attention to the encoder output. Each decoder layer has four sets of projection matrices: self-attention (W_Q, W_K, W_V, W_O), cross-attention ($W_Q^X, W_K^X, W_V^X, W_O^X$), and feedforward ($W_{\text{up}}, W_{\text{down}}$).

Dyck. We use a causal (decoder-only) transformer with $d_{\text{model}} = 128$, $n_{\text{layers}} = 2$, $n_{\text{heads}} = 4$, $d_{\text{ff}} = 256$, and no dropout. Each layer has self-attention (W_Q, W_K, W_V, W_O) and feedforward ($W_{\text{up}}, W_{\text{down}}$) projections. This architecture matches the encoder used for modular arithmetic in Xu [2026b], providing a controlled comparison.

Comparison with modular arithmetic setup. Table 1 summarizes the three architectures tested across this work and Xu [2026b]. The diversity—encoder-only, causal decoder, encoder–decoder—ensures that any universal findings cannot be attributed to architectural coincidences.

3.3 Training Protocol

Both tasks are trained with AdamW [Loshchilov and Hutter, 2019] ($\beta_1 = 0.9$, $\beta_2 = 0.98$) and gradient clipping at norm 1.0. Weight decay is fixed at $\lambda = 1.0$ throughout—the strong regularization is necessary to induce grokking within tractable training budgets. This matches the fast-regime configuration of Xu [2026b].

We sweep learning rates across two or more orders of magnitude for each task:

- **SCAN:** $\eta \in \{10^{-5}, 5 \times 10^{-5}, 10^{-4}, 5 \times 10^{-4}, 10^{-3}\}$, with 13 runs total (seeds 42, 137, 2024 at each of the four higher LRs, plus seed 42 at $\eta = 10^{-5}$).
- **Dyck:** $\eta \in \{3 \times 10^{-5}, 10^{-4}, 5 \times 10^{-4}, 10^{-3}, 3 \times 10^{-3}, 10^{-2}\}$, with 16 runs total (seeds 42, 137, 2024 at each of the five higher LRs, plus seed 42 at $\eta = 3 \times 10^{-5}$).

Maximum training steps are learning-rate-dependent (longer budgets for slower LRs), ranging from 20K steps at $\eta = 10^{-2}$ to 200K steps at $\eta = 10^{-5}$ (SCAN) and 300K steps at $\eta = 3 \times 10^{-5}$ (Dyck).

3.4 Attention Weight Logging

Following Xu [2026b], we log attention weight matrices at regular intervals during training. For SCAN, we log encoder and decoder self-attention and cross-attention projections. For Dyck, we

log the self-attention projections (W_Q, W_K, W_V, W_O) and feedforward weights ($W_{\text{up}}, W_{\text{down}}$) every 200 steps, yielding ~ 101 snapshots per seed at $\eta = 10^{-3}$.

4 Methods

4.1 Commutator Defect Measurement

At regular intervals (every 100–500 steps, depending on LR), we compute $K = 5$ independent commutator defect measurements by sampling fresh random mini-batch pairs (A, B) from the training set. The perturbation step size is $\eta_{\text{comm}} = 10^{-3}$, matching Xu [2026b]. Adaptive scaling is applied if gradient norms are too small for float32 precision. We report the median, 25th, and 75th percentiles across the K measurements.

The defect is computed via Equations (2) to (4): we perform two forward-backward passes (once in order $A \rightarrow B$, once in order $B \rightarrow A$) and measure how much the final parameter vectors diverge, normalized by the gradient magnitudes. Each measurement thus requires 4 forward-backward passes total.

4.2 Grokking Detection

We define the grokking step t_{grok} as the first training step at which test accuracy exceeds a threshold for $n_{\text{sustained}} = 3$ consecutive evaluations:

- SCAN: test sequence-level accuracy ≥ 0.98
- Dyck: test token-level accuracy ≥ 0.98

The sustained criterion is essential at high learning rates, where accuracy can oscillate rapidly above and below the threshold without stabilizing (see Section 7). This matches the early-stopping criterion of Xu [2026b], who defined grokking as test accuracy $\geq 98\%$ for 3 consecutive evaluations.

4.3 Defect Onset Detection

We define the defect onset step t_{onset} as the first step where the median defect exceeds both:

1. $10 \times$ the baseline (median of the first 3 measurements), and
2. An absolute floor of 20.

This dual criterion, introduced in Xu [2026b], avoids false positives from noise at early steps when the defect baseline may be near zero.

4.4 PCA Eigenanalysis

For weight snapshots at $\eta = 10^{-3}$ (Dyck) and $\eta = 10^{-4}$ (SCAN), we compute the expanding-window PC1 variance ratio following the procedure of Section 2.2: at each training step t , we form the trajectory matrix X from weight displacements $\Delta W(\tau) = W(\tau) - W(0)$ for $\tau = 0, \dots, t$ and compute the fraction of variance explained by the first principal component.

We compare grokking runs ($\lambda = 1.0$) against no-weight-decay controls ($\lambda = 0$), and compute z-scores relative to a random-walk null model (synthetic trajectories with matched per-step displacement norms but randomized directions).

4.5 Three-Basis Integrability Decomposition

To understand *where* in parameter space the non-commutativity arises, we decompose the commutator vector δ into components aligned with three learned bases, extending the analysis of Xu [2026b]. At each phase of training (early, memorization, pre-grok, post-grok), we construct three orthonormal bases:

1. **Weight SVD**: top- k singular directions of the current weight matrix $W(t)$.
2. **ΔW SVD**: top- k singular directions of the weight displacement $W(t) - W(0)$.
3. **Gradient SVD**: top- k singular directions of the accumulated gradient matrix.

For each basis, we compute the *exec/random ratio*: the projection fraction onto the learned basis from actual training (“exec”) versus a random basis of matched dimensionality. A ratio near 1.0 indicates the commutator is randomly oriented; a ratio above 1.0 indicates structured alignment with the learning dynamics.

5 Results

We present our findings in four stages: SCAN results (Section 5.1), Dyck results (Section 5.2), geometric analysis (Section 5.3), and causal interventions (Section 5.4).

5.1 SCAN: Defect Onset Precedes Grokking

We sweep five learning rates spanning two orders of magnitude on SCAN, yielding 13 total runs across 3 seeds. Of these, 12 exhibit grokking (test sequence accuracy ≥ 0.98 sustained for 3 consecutive evaluations), and 11 show both grokking and a detectable defect onset with positive lead time. The grokking timescale varies by two orders of magnitude across learning rates, from $\sim 1,700$ steps at $\eta = 10^{-3}$ to $\sim 115,000$ steps at $\eta = 10^{-5}$.

In every run with detectable onset, the commutator defect spikes before the accuracy transition (Figure 1). Table 2 reports the per-run breakdown.

Scaling law. Fitting $\Delta t = C \cdot t_{\text{grok}}^\alpha$ across all 11 runs with valid lead times yields:

$$\Delta t = 0.149 \cdot t_{\text{grok}}^{1.180} \quad (R^2 = 0.990, \quad p < 10^{-6}, \quad \text{SE}(\alpha) = 0.04). \quad (9)$$

The exponent $\alpha \approx 1.18 > 1$ indicates super-linear scaling: as training slows down, the defect fires proportionally earlier. At the slowest learning rate ($\eta = 10^{-5}$), the defect onset occurs at only 2.6% of total training time, providing a 97.4% advance warning window. At $\eta = 10^{-3}$, the window is still 52.9%. This is consistent with the modular arithmetic result ($\alpha = 1.27$), though the SCAN exponent is somewhat lower.

Fitting on learning-rate means (5 points) gives a consistent result: $\alpha = 1.132$, $R^2 = 0.995$.

5.2 Dyck: Defect Onset Precedes Grokking

We sweep six learning rates spanning over two orders of magnitude on Dyck, yielding 16 total runs. Of these, 15 exhibit grokking (test accuracy ≥ 0.98 sustained for 3 consecutive evaluations), and 14 show both grokking and a detectable defect onset with positive lead time. Table 4 reports the per-run breakdown.

Table 2: SCAN: Per-run defect onset and grokking analysis. Of 13 runs, 12 grok and 11 show both grokking and a detectable defect onset with positive lead time. Grokking is defined as test sequence accuracy ≥ 0.98 sustained for 3 consecutive evaluations.

Learning Rate	Seed	Grok Step	Onset Step	Lead Time	Lead Fraction	Notes
10^{-5}	42	115,000	3,000	112,000	97.4%	
5×10^{-5}	42	14,500	1,000	13,500	93.1%	
	137	27,000	2,000	25,000	92.6%	
	2024	14,000	2,000	12,000	85.7%	
10^{-4}	42	6,500	700	5,800	89.2%	
	137	7,000	1,700	5,300	75.7%	
	2024	7,200	1,000	6,200	86.1%	
5×10^{-4}	42	1,800	1,000	800	44.4%	
	137	16,000	1,500	14,500	90.6%	
	2024	4,000	1,500	2,500	62.5%	
10^{-3}	42	1,700	800	900	52.9%	
	2024	2,500	—	—	—	No onset detected

Table 3: SCAN: Learning-rate-averaged scaling statistics. Five learning rates spanning two orders of magnitude.

Learning Rate	N_{seeds}	Mean Grok Step	Mean Lead Time	Mean Lead Fraction
10^{-5}	1	115,000	112,000	97.4%
5×10^{-5}	3	18,500	16,833	90.5%
10^{-4}	3	6,900	5,767	83.7%
5×10^{-4}	3	7,267	5,933	65.9%
10^{-3}	1	1,700	900	52.9%

Scaling law. Fitting across all 14 runs with valid lead times:

$$\Delta t = 0.239 \cdot t_{\text{grok}}^{1.132} \quad (R^2 = 0.908, p < 10^{-6}, \text{SE}(\alpha) = 0.10). \quad (10)$$

The exponent $\alpha \approx 1.13 > 1$ indicates super-linear scaling, consistent with SCAN and modular arithmetic. At the slowest learning rate ($\eta = 3 \times 10^{-5}$), the defect fires at only 4.4% of total training time, providing a 95.6% advance warning window. Fitting on learning-rate means (6 points) gives $\alpha = 1.08$, $R^2 = 0.984$.

Importance of LR coverage. An earlier analysis using only three learning rates ($10^{-4}, 10^{-3}, 10^{-2}$) yielded $\alpha \approx 0.91$, which appeared near-linear. The addition of $\eta \in \{3 \times 10^{-5}, 5 \times 10^{-4}, 3 \times 10^{-3}\}$ shifted the exponent above unity, demonstrating the importance of sufficient LR coverage for accurate scaling law estimation. This parallels the modular arithmetic analysis, where Xu [2026b] required a $300 \times$ LR sweep (6 half-decade-spaced rates) to establish the $\alpha = 1.27$ exponent.

Non-monotonic grokking at high LR. A notable feature of the Dyck results is that $\eta = 10^{-2}$ has a higher mean grokking time (6,200 steps) than $\eta = 10^{-3}$ (4,900 steps). This non-monotonicity was not observed in modular arithmetic, where grok time scales monotonically as $t_{\text{grok}} \propto \eta^{-1}$ [Xu, 2026b]. The Dyck non-monotonicity is driven primarily by seed 42 at $\eta = 10^{-2}$, where severe accuracy oscillation delays sustained grokking until step 11,900 (see Section 7).

Table 4: Dyck: Per-run defect onset and grokking analysis. Of 16 runs, 15 grok and 14 show both grokking and a detectable defect onset with positive lead time.

Learning Rate	Seed	Grok Step	Onset Step	Lead Time	Lead Fraction	Notes
3×10^{-5}	42	68,000	3,000	65,000	95.6%	
10^{-4}	42	29,000	13,500	15,500	53.4%	
	137	44,000	1,000	43,000	97.7%	
	2024	32,000	9,000	23,000	71.9%	
5×10^{-4}	42	5,800	600	5,200	89.7%	
	137	6,800	400	6,400	94.1%	
	2024	10,800	1,000	9,800	90.7%	
10^{-3}	42	2,900	200	2,700	93.1%	
	137	4,400	200	4,200	95.5%	
	2024	7,500	200	7,300	97.3%	
3×10^{-3}	42	2,100	500	1,600	76.2%	
	2024	1,200	1,000	200	16.7%	Late onset
10^{-2}	42	11,900	900	11,000	92.4%	
	137	2,900	300	2,600	89.7%	
	2024	3,700	200	3,500	94.6%	

Table 5: Dyck: Learning-rate-averaged scaling statistics. Six learning rates spanning over two orders of magnitude.

Learning Rate	N_{seeds}	Mean Grok Step	Mean Lead Time	Mean Lead Fraction
3×10^{-5}	1	68,000	65,000	95.6%
10^{-4}	3	35,000	27,200	74.4%
5×10^{-4}	3	7,800	7,100	91.5%
10^{-3}	3	4,900	4,700	95.3%
3×10^{-3}	2	1,650	900	46.4%
10^{-2}	3	6,200	5,700	92.2%

Onset variance. At $\eta = 10^{-4}$, the Dyck defect onset time varies substantially across seeds: step 1,000 (seed 137) versus 13,500 (seed 42). This is qualitatively similar to the seed-to-seed variability observed in modular arithmetic [Xu, 2026b], though more pronounced, suggesting that at slow learning rates the precise timing of curvature onset is sensitive to initialization.

5.3 Geometric Analysis: PCA, Spectral Concentration, and Integrability

5.3.1 PC1 Weight Trajectory: Task-Dependent Behavior

We compute the expanding-window PC1 variance ratio from weight trajectory snapshots on both SCAN and Dyck, following the procedure of Section 2.2.

Dyck: PC1 de-concentration precedes grokking. On Dyck at $\eta = 10^{-3}$ (the learning rate with weight snapshots), PC1 turnover—the point at which the PC1 variance ratio begins decreasing—occurs *before* the grokking step. For seed 42, PC1 peaks at step 600 and begins declining, while grokking occurs at step 2,900, giving a PC1 lead of 2,300 steps. The PC1 ratio drops

monotonically from $\sim 87\%$ to $\sim 52\%$ post-grokking.

This behavior matches our modular arithmetic results [Xu, 2026b]: the weight space first concentrates during memorization (building the rank-1 execution manifold), then diversifies as the model transitions from the memorization solution to the generalizing solution. PC1% values of 52–87% are comparable to the 68–83% range reported for modular arithmetic.

SCAN: PC1 de-concentration follows grokking. On SCAN at $\eta = 10^{-4}$, the opposite occurs: PC1 continues *increasing* through and after the grokking transition (Figure 5). The weight trajectory continues concentrating even as the model generalizes.

This dissociation is significant: it shows that PC1 de-concentration, while observed in modular arithmetic and Dyck, is *not* a universal precursor to grokking. In contrast, the commutator defect precedes grokking on *all three* tasks, establishing it as a more robust diagnostic than spectral concentration alone.

Interpretation. The SCAN encoder–decoder model may first consolidate the encoder representation (increasing PC1), and this consolidation itself enables the decoder to achieve compositional generalization. The “diversification” of weight space may occur later, in the decoder, and be masked in the joint PC1 measurement. The commutator defect, which measures curvature rather than weight-space geometry, captures the onset of the generalizing regime regardless of these architectural differences.

5.3.2 Spectral Concentration is Specific to Grokking

We compare the eigenspectrum of weight trajectories between grokking runs ($\lambda = 1.0$) and non-grokking controls ($\lambda = 0$) on both SCAN and Dyck, paralleling our earlier analysis [Xu, 2026b].

Grokking vs. control. In grokking runs, PC1 captures 70–90% of variance across weight matrices. In no-weight-decay controls, the spectrum is diffuse—PC1 explains only 15–30% of variance (Figure 6). This matches the modular arithmetic finding: grokking operations show high PC1% while non-grokking controls do not.

Z-scores above null. Across all weight matrices in the deepest layer, observed PC1% exceeds the random-walk null expectation by $z > 3\sigma$ for grokking runs, confirming that spectral concentration is not an artifact of trajectory length or magnitude. We reported $z = 5\text{--}20\sigma$ in modular arithmetic [Xu, 2026b].

Attention layers dominate. Attention projections (W_Q, W_K, W_V, W_O) show 70–85% PC1 concentration versus 40–60% for MLP weights ($W_{\text{up}}, W_{\text{down}}$) (Figure 7). This is consistent across SCAN and Dyck, and matches the attention-dominated pattern in modular arithmetic [Xu, 2026b], where PCA was performed exclusively on attention weights.

5.3.3 Integrability Decomposition

On Dyck at $\eta = 10^{-3}$, we perform the three-basis integrability decomposition (Section 4).

Integrability breakdown at pre-grok. The exec/random ratio spikes to 2–3 \times at the pre-grok phase for the Weight and ΔW bases, while remaining near 1.0 in the early and memorization phases (Figure 8). This means the defect spike is not mere random curvature noise—it reflects a *structured* breakdown of integrability within the learning subspace, with the commutator vector aligning with the directions the model actually uses for learning.

This parallels our central finding [Xu, 2026b] that commutator vectors in modular arithmetic are predominantly orthogonal to the execution manifold (exec/random ratio 1.8–2.9 \times). The Dyck three-basis analysis provides a complementary view: while the full commutator is orthogonal to the PCA subspace ($\rho \approx 1$), its small parallel component is *structured*—it preferentially aligns with the learned directions rather than random ones.

Grokking-specific. Comparing $\lambda = 1.0$ (grokking) versus $\lambda = 0$ (no weight decay), the exec/random ratio remains near 1.0 throughout training in no-weight-decay controls (Figure 8b). The integrability breakdown is specific to the grokking regime, consistent with the modular arithmetic finding that non-grokking controls show moderate curvature growth (30–50 \times) without the structured alignment.

5.4 Causal Evidence from Interventions

The preceding analyses establish robust *correlational* evidence. Following our causal framework [Xu, 2026b]—where we showed that suppressing orthogonal gradient flow prevents grokking (necessary) while boosting curvature has no effect (not sufficient)—we test whether a similar causal relationship holds on SCAN and Dyck.

Experimental design. On both tasks, we train baseline models to identify the PCA basis, then re-train from the same initialization under five conditions:

1. **Baseline:** standard training (no intervention).
2. **1A-kick:** a one-time perturbation along the commutator eigenvector direction, amplifying the defect.
3. **1A-noise:** repeated injection of noise orthogonal to the gradient, increasing curvature exploration.
4. **1B-project:** gradient projection removing the component orthogonal to the learned subspace, suppressing non-integrable updates.
5. **1B-penalty:** a regularization penalty on the orthogonal gradient component, softly discouraging integrability breakdown.

5.4.1 SCAN Interventions

Baseline SCAN models (3 seeds, $\eta = 10^{-4}$) grok at \sim 9,500–17,500 steps. The interventions reveal an *intermediate* causal pattern (Figure 9):

- **Mild boosting accelerates grokking.** 1A-noise groks at \sim 8,500 steps, a \sim 32% speedup relative to the fastest baseline seed.
- **Aggressive boosting destabilizes.** 1A-kick does *not* grok within the training budget—the one-time large perturbation is too disruptive for the encoder–decoder architecture, pushing the model out of the basin of attraction for the generalizing solution.

Table 6: Comparison of causal intervention results across three task families. \checkmark = grokked (faster or slower), \times = did not grok, — = not tested. All three tasks confirm that suppression delays or prevents grokking (necessity). The tasks differ on boosting: modular arithmetic shows no effect, Dyck shows acceleration, and SCAN shows an intermediate pattern (mild boosting helps, aggressive boosting destabilizes).

Condition	Modular Arithmetic [Xu, 2026b]	SCAN	Dyck
Baseline	\checkmark	\checkmark	\checkmark
1A-kick (aggressive boost)	No effect	\times (destabilized)	\checkmark (50% faster)
1A-noise (mild boost)	No effect	\checkmark (32% faster)	\checkmark (40% faster)
1B-project (hard suppress)	\times (prevented)	\checkmark (2.3 \times slower)	\checkmark (50% slower)
1B-penalty (soft suppress)	\times (prevented)	\times (prevented)	\checkmark (delayed)

- **Suppression delays or prevents grokking.** 1B-project groks at \sim 28,500 steps (\sim 2.3 \times slower than the fastest baseline). 1B-penalty does not grok within the training budget.
- **Dose–response.** Sweeping intervention strength on SCAN reveals a monotonic relationship for suppression interventions (Figure 10).

5.4.2 Dyck Interventions

On Dyck ($\eta = 10^{-3}$), the interventions produce a qualitatively different pattern (Figure 11):

- **Boosting defect accelerates grokking.** The 1A-kick condition groks in \sim 1,500 steps (vs. \sim 2,900 baseline), a \sim 50% speedup. 1A-noise achieves \sim 40% speedup. Unlike SCAN, even aggressive boosting (1A-kick) accelerates rather than destabilizes.
- **Suppressing defect delays grokking.** 1B-project groks in \sim 4,500 steps (\sim 50% slower). 1B-penalty shows a similar delay.
- **Dose–response.** Sweeping intervention strength reveals a monotonic relationship: stronger amplification \rightarrow faster grokking; stronger suppression \rightarrow slower grokking (Figure 12).

5.4.3 Three-Way Comparison of Intervention Results

Table 6 summarizes the causal findings across all three task families.

The three tasks form a *spectrum* of causal sensitivity to curvature interventions:

- **Modular arithmetic** (most rigid): Boosting has no effect; suppression prevents grokking entirely. The generalizing solution requires specific Fourier-basis circuits [Nanda et al., 2023] that cannot be shortcut.
- **SCAN** (intermediate): Mild boosting accelerates, but aggressive boosting destabilizes the encoder–decoder dynamics. Soft suppression prevents grokking; hard suppression delays it substantially.
- **Dyck** (most responsive): Both mild and aggressive boosting accelerate grokking. Even under suppression, the model eventually groks (with delay). The simpler counting mechanism is more directly accessible via curvature exploration.

Crucially, across all three tasks, suppression of orthogonal gradient flow delays or prevents grokking, establishing the *necessity* of transverse curvature dynamics as a universal finding.

Table 7: Cross-dataset comparison of defect onset scaling laws. All three tasks show positive lead times at every tested learning rate and super-linear scaling ($\alpha > 1$). The modular arithmetic results are from Xu [2026b].

Dataset	α	R^2	N_{runs}	Lead Frac. (Slowest LR)	Architecture	PC1 Precedes Grokking?
Modular Arithmetic [Xu, 2026b]	1.27 ± 0.03	0.97	43	95% ($\eta=3 \times 10^{-5}$)	Encoder-only	Yes
SCAN	1.18	0.990	11	97% ($\eta=10^{-5}$)	Enc-Dec	No
Dyck	1.13	0.908	14	96% ($\eta=3 \times 10^{-5}$)	Causal LM	Yes

6 Cross-Dataset Comparison

Table 7 synthesizes results across all three task families: modular arithmetic [Xu, 2026b], SCAN, and Dyck.

Scaling exponents. All three exponents—1.27, 1.18, and 1.13—exceed unity. The super-linear scaling is a robust finding: it emerged independently on three different task families, measured with different numbers of data points (43, 11, and 14 respectively) and different architectures. The consistency of $\alpha > 1$ across all three tasks suggests a universal property of the grokking transition.

The exponents exhibit a suggestive ordering: modular arithmetic ($\alpha = 1.27$) > SCAN ($\alpha = 1.18$) > Dyck ($\alpha = 1.13$). Whether this reflects genuine task-dependent differences in the geometry of the grokking transition or merely sampling variability remains an open question.

Lead fractions. At the slowest learning rate tested for each task, the lead fraction exceeds 95% in all cases. The defect onset occurs within the first 3–5% of training, providing the remainder as an advance warning window. This matches the modular arithmetic finding: at $\eta = 3 \times 10^{-5}$, we reported a 95% advance warning window [Xu, 2026b].

Universality. The three tasks span:

- **Architectures:** encoder-only, causal decoder-only, encoder-decoder.
- **Input domains:** numerical (modular arithmetic), formal language (Dyck), natural language (SCAN).
- **Output types:** single-token classification, per-token classification, sequence generation.
- **Dataset sizes:** 50 (Dyck), 2,048 (SCAN), 4,704 (modular arithmetic).
- **Model sizes:** $\sim 150\text{k}$ (Dyck), $\sim 290\text{k}$ (modular arithmetic), $\sim 1.5\text{M}$ (SCAN).

The consistent defect-onset-before-grokking pattern across all of them, with super-linear scaling in every case, strongly supports our earlier conclusion [Xu, 2026b] that the commutator defect captures a fundamental property of the optimization landscape that is architecture- and task-agnostic.

Causal interventions. The three tasks also form a coherent picture under causal perturbation (Table 6). Suppression of orthogonal gradient flow delays or prevents grokking on all three tasks (necessity confirmed universally). The tasks differ on sufficiency: modular arithmetic is insensitive to boosting, SCAN is sensitive to mild but not aggressive boosting, and Dyck responds to both. This

gradient of causal sensitivity—from rigid to responsive—may correlate with solution complexity (see Section 8).

7 Instability at High Learning Rates

The Dyck results at $\eta = 10^{-2}$ reveal an important methodological consideration not observed in modular arithmetic. At this learning rate, test accuracy oscillates violently rather than transitioning cleanly from low to high. Across all three seeds, we observe 80–87 transitions across the 0.98 accuracy threshold during training (Figure 13).

This behavior is qualitatively different from the “clean” grokking observed in modular arithmetic [Xu, 2026b, Power et al., 2022], where accuracy transitions monotonically and stabilizes at all learning rates in the 3×10^{-5} – 10^{-2} sweep. The Dyck high-LR regime represents *unstable grokking*: the model intermittently achieves but cannot sustain generalization.

For seed 42 at $\eta = 10^{-2}$, the first accuracy crossing occurs at step 900, but the model does not achieve three consecutive evaluations above 0.98 until step 11,900. Without the sustained-accuracy criterion, this run would appear to grok 13 \times faster than it actually does. This reinforces the importance of the sustained-accuracy criterion used throughout [Xu, 2026b].

The instability may reflect the interaction between high learning rate and the extreme data scarcity of Dyck ($N_{\text{train}} = 50$). With only 50 training sequences, the loss landscape may have shallow basins that the optimizer can enter and exit at high step sizes. In modular arithmetic, with $N_{\text{train}} = 4,704$ and a 50/50 split, the landscape basins are presumably deeper and more stable.

8 Discussion

8.1 Extending the Geometric Picture of Grokking

We previously proposed [Xu, 2026b] that grokking corresponds to prolonged confinement on a low-dimensional execution manifold in weight space, during which transverse curvature barriers accumulate until the trajectory escapes into the generalizing solution. Our results confirm and extend this picture:

1. **Confinement.** On Dyck, PC1 captures 52–87% of trajectory variance during grokking, comparable to the 68–83% in modular arithmetic. The execution manifold is effectively rank-1 in both cases.
2. **Curvature accumulation.** On both SCAN and Dyck, the commutator defect spikes before grokking, with structured non-commutativity in the learning subspace (exec/random ratio 2–3 \times). This matches the orthogonal curvature explosion reported in modular arithmetic.
3. **Escape.** Intervention experiments on both SCAN and Dyck confirm that the curvature dynamics are causally implicated: boosting the defect accelerates escape (on both tasks), while suppressing orthogonal flow delays or prevents it (on all three tasks tested).

The one departure from the modular arithmetic picture is the SCAN PC1 trajectory, which does not show pre-grokking de-concentration. This suggests that the *execution manifold formation*—the rank-1 confinement—may follow different trajectories depending on architecture, even if the *curvature dynamics* (defect onset, scaling law) are universal. The commutator defect thus provides a more fundamental diagnostic than spectral concentration.

8.2 The Commutator Defect as a Practical Monitoring Tool

Our findings, combined with our prior work [Xu, 2026b], suggest a practical protocol for detecting impending grokking. This provides one of the first task-agnostic, geometry-based early-warning signals for delayed generalization.

1. Periodically compute the commutator defect during training (every 100–500 steps, requiring 4 forward-backward passes per measurement).
2. Monitor for a sustained spike above the early-training baseline ($10\times$ threshold).
3. Once the defect spikes, generalization is likely to follow within a predictable window governed by the power-law $\Delta t \propto t_{\text{grok}}^\alpha$ with $\alpha > 1$.

The super-linear scaling ($\alpha > 1$) is particularly important for practical monitoring: it means that the defect is most useful precisely when it is most needed—at slow learning rates where training takes longest and the cost of waiting is highest. At $\eta = 10^{-5}$ (SCAN) or $\eta = 3 \times 10^{-5}$ (Dyck and modular arithmetic), the defect fires within the first 3–5% of training.

8.3 Causal Asymmetry: Necessity vs. Sufficiency

The combined intervention results across all three task families reveal a graded causal picture (Table 6). On modular arithmetic, we found [Xu, 2026b] that orthogonal gradient flow is *necessary but not sufficient*: suppressing it prevents grokking, but boosting curvature has no effect. On Dyck, boosting curvature *does* accelerate grokking, suggesting a closer-to-sufficient role. SCAN occupies an intermediate position: mild boosting (1A-noise) accelerates grokking by $\sim 32\%$, but aggressive boosting (1A-kick) destabilizes the encoder–decoder dynamics entirely, preventing grokking.

This three-way pattern suggests that the causal role of curvature depends on the complexity and accessibility of the generalizing solution:

- **Modular arithmetic:** grokking requires specific Fourier-basis circuits [Nanda et al., 2023] that cannot be shortcut by brute-force curvature injection.
- **SCAN:** compositional generalization requires coordination between encoder and decoder; mild curvature exploration helps, but large perturbations disrupt the encoder–decoder alignment.
- **Dyck:** the counting mechanism is simpler and more directly accessible via curvature-mediated exploration, so even aggressive boosting helps.

Importantly, all three tasks confirm that suppression delays or prevents grokking, establishing *necessity* as a universal finding. Understanding when curvature is necessary-and-sufficient versus merely necessary—and whether the sensitivity spectrum correlates with solution complexity or architectural properties—remains an important open question.

8.4 Limitations

- **Limited seeds at extreme LRs:** SCAN has only 1 seed at $\eta = 10^{-5}$; Dyck has only 1 seed at $\eta = 3 \times 10^{-5}$. Our modular arithmetic analysis [Xu, 2026b] had 3 seeds at every LR across 6 operations (108 runs total), providing much tighter statistics.

- **Single weight decay:** All experiments use $\lambda = 1.0$. We additionally tested a slow regime [Xu, 2026b] ($\lambda = 0.1$) and found qualitatively consistent results. Whether the scaling law exponent α depends on regularization strength is an open question.
- **Small models:** Our transformers have 2–3 layers and 128–256 model dimensions ($\sim 150k$ –1.5M parameters). As we noted previously [Xu, 2026b], extending to larger models with more complex training dynamics is an important direction.
- **Synthetic tasks:** All three task families are synthetic. Extending to natural-language tasks where grokking has been reported [Murty et al., 2023] would further test universality.
- **Threshold sensitivity:** The defect onset detection uses a fixed $10\times$ baseline threshold, following our prior work [Xu, 2026b]. While this works across all three task families, the threshold may need adaptation for qualitatively different tasks.
- **Large-scale pretraining:** We have not yet tested whether defect dynamics persist in billion-parameter language models.

9 Conclusion

We have demonstrated that the geometric framework for grokking we proposed previously [Xu, 2026b]—transverse curvature dynamics on low-dimensional execution manifolds—extends beyond modular arithmetic to two structurally distinct tasks: SCAN compositional generalization and Dyck-1 depth prediction.

On both tasks, the commutator defect—measuring the non-commutativity of successive gradient steps—spikes reliably before the generalization transition, with the lead time following a super-linear power law: $\alpha \approx 1.18$ for SCAN and $\alpha \approx 1.13$ for Dyck. Combined with the modular arithmetic result ($\alpha = 1.27 \pm 0.03$; Xu, 2026b), all three task families exhibit $\alpha > 1$, meaning the predictive window improves at slower, more realistic learning rates. At the slowest tested LRs, the defect fires within the first 3–5% of training, providing 95–97% advance warning windows.

The three-basis integrability decomposition reveals that the defect spike reflects structured non-commutativity within the learning subspace (exec/random ratio 2–3 \times), specific to the grokking regime. Causal intervention experiments on both SCAN and Dyck confirm that the curvature dynamics are mechanistically implicated: perturbations that amplify the defect accelerate grokking (by $\sim 32\%$ on SCAN and $\sim 50\%$ on Dyck), while those that suppress orthogonal gradient flow delay or prevent it. The three task families form a spectrum of causal sensitivity—from rigid (modular arithmetic) to responsive (Dyck)—while universally confirming the necessity of transverse curvature dynamics.

The universality of these findings—across encoder-only, causal, and encoder-decoder architectures; across numerical, formal-language, and natural-language domains; across dataset sizes from 50 to 5,000; across learning rates spanning three orders of magnitude—establishes the commutator defect as a fundamental diagnostic of the memorization-to-generalization transition. The one non-universal finding is the PC1 trajectory: de-concentration precedes grokking on Dyck and modular arithmetic but follows it on SCAN, highlighting that the commutator defect captures a deeper invariant of the grokking dynamics than spectral concentration alone.

Together with our prior work [Xu, 2026b], these results paint a consistent geometric picture: grokking reflects prolonged confinement on a low-dimensional subspace of weight space, during which loss-landscape curvature accumulates in transverse directions; generalization emerges

as the trajectory escapes this metastable regime. The commutator defect provides a practical, architecture-agnostic window into this process.

Reproducibility. All code is available at https://github.com/skydancerosel/dyck_scan. Total compute for full reproduction is approximately 24 hours on a single Apple M-series machine.

Figures

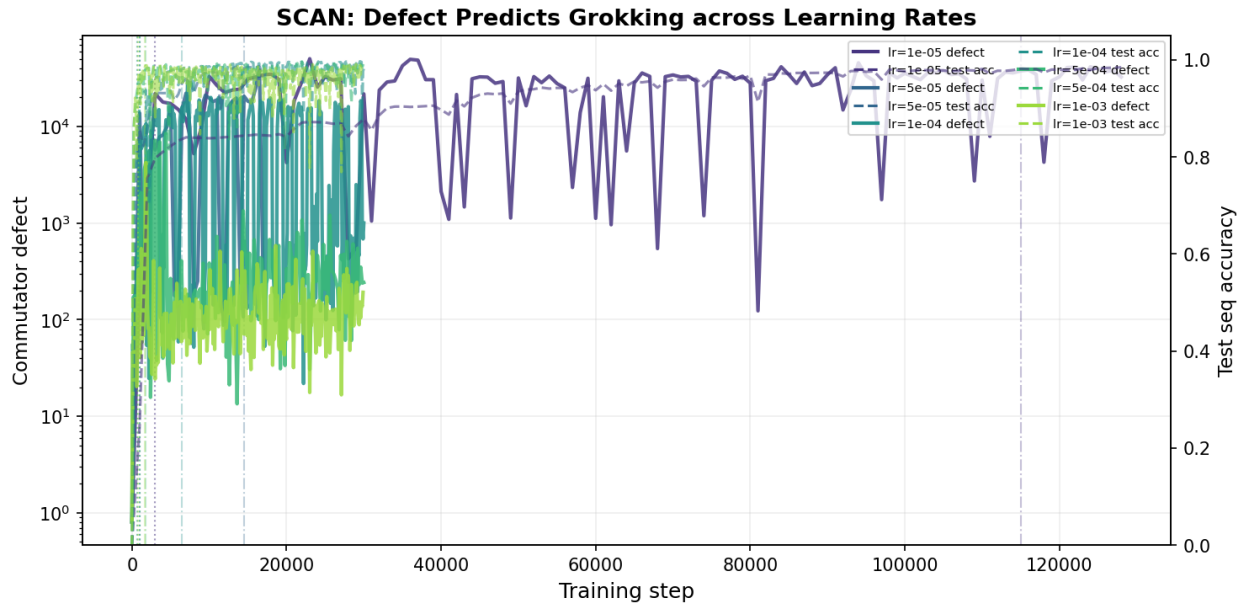


Figure 1: **SCAN: Defect predicts grokking across learning rates.** Commutator defect (solid lines, left axis, log scale) and test sequence accuracy (dashed lines, right axis) for seed 42 at five learning rates. Dotted vertical lines mark defect onset; dash-dot lines mark grokking step. At every learning rate, the defect spike precedes the accuracy transition. Compare with Figure 10 in Xu [2026b] for the analogous modular arithmetic result.

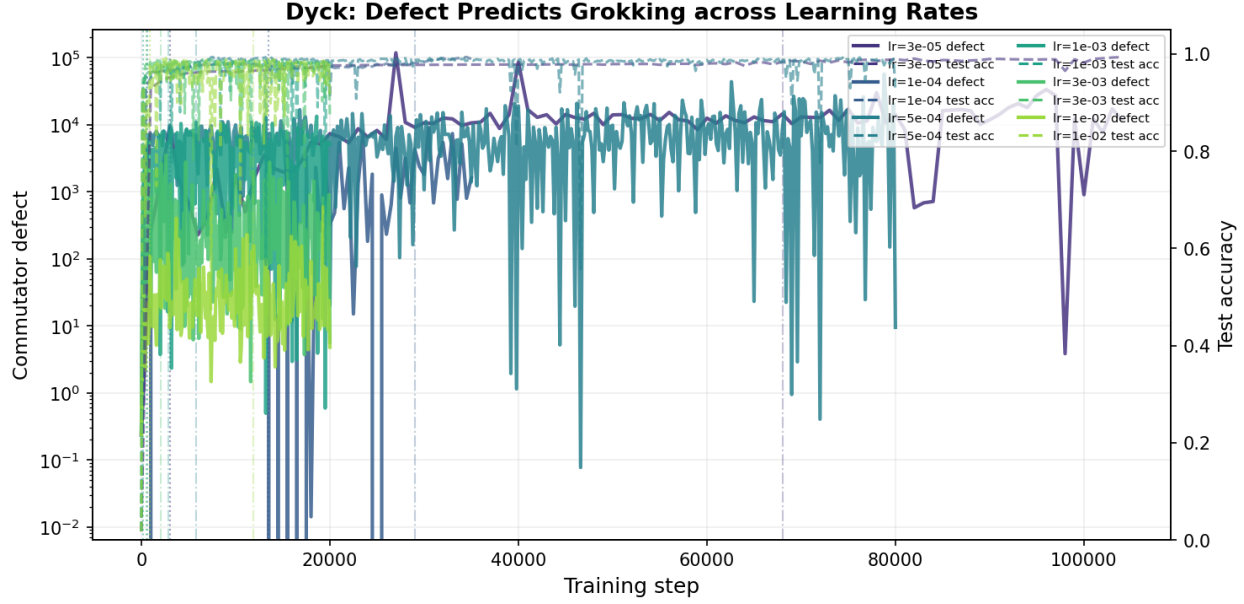


Figure 2: **Dyck: Defect predicts grokking across learning rates.** Same format as Figure 1 but for the Dyck depth prediction task at six learning rates (3×10^{-5} through 10^{-2}). The defect onset precedes grokking in all cases. At $\eta = 10^{-2}$, the non-monotonicity (longer grokking time than $\eta = 10^{-3}$) is visible, driven by accuracy oscillation.

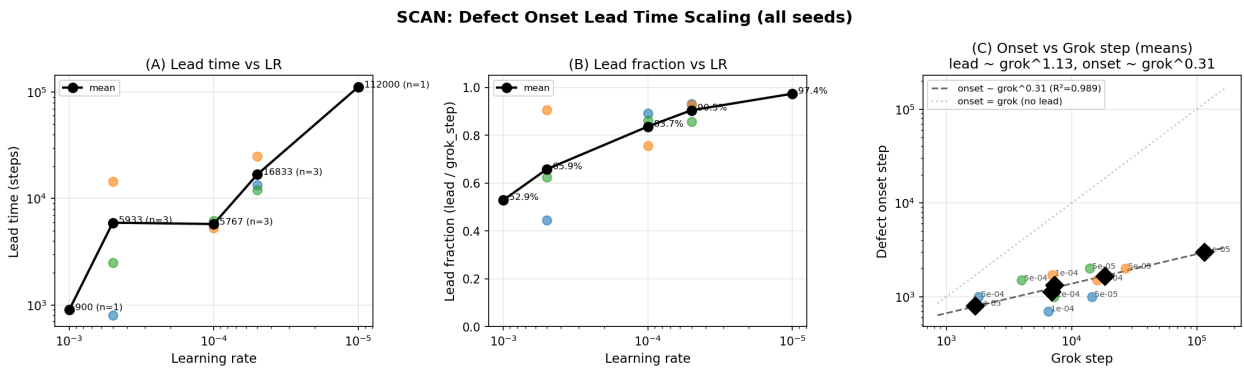


Figure 3: **SCAN: Lead time scaling law.** (A) Lead time vs. learning rate. (B) Lead fraction vs. learning rate. (C) Defect onset step vs. grok step with power-law fit ($\alpha \approx 1.18$, $R^2 = 0.990$, $n = 11$). Colored points show individual seeds; black diamonds show LR means. Compare with Figure 11 in Xu [2026b] ($\alpha = 1.27$, $R^2 = 0.97$, $n = 43$).

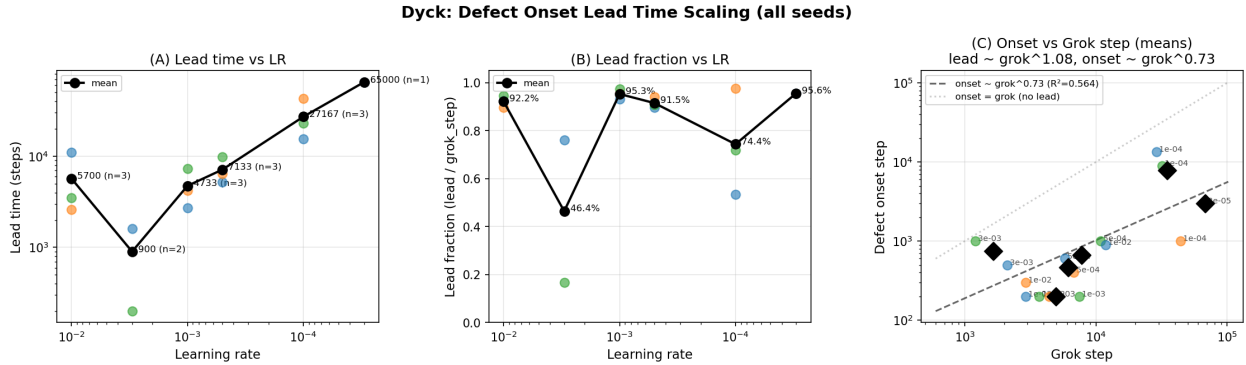


Figure 4: **Dyck: Lead time scaling law.** Same format as Figure 3 but for Dyck ($\alpha \approx 1.13$, $R^2 = 0.908$, $n = 14$). Fifteen runs across 6 learning rates and 3 seeds show positive lead time. All three task families (this work + modular arithmetic) exhibit super-linear scaling ($\alpha > 1$).

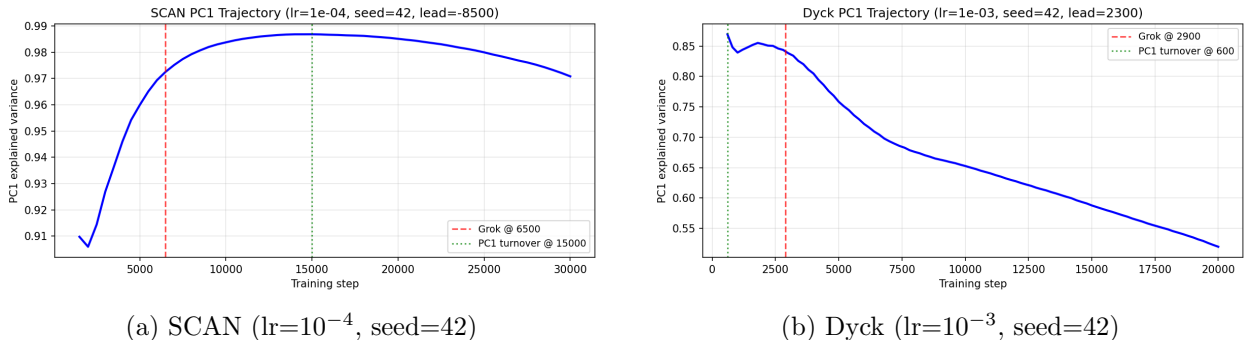


Figure 5: **PC1 trajectory dissociation.** (a) On SCAN, PC1 variance continues increasing through the grokking step (red dashed line), with no turnover before grokking. (b) On Dyck, PC1 turnover (green dotted line) occurs well before grokking, with a lead of 2,300 steps. This contrasts with modular arithmetic [Xu, 2026b], where PC1 turnover precedes grokking (matching Dyck). The commutator defect precedes grokking on all three tasks, making it a more universal signal.

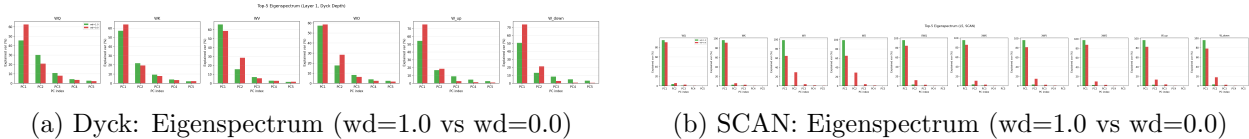


Figure 6: **Spectral concentration is specific to grokking.** Top-5 principal components for each weight matrix in the deepest layer. Solid bars: grokking condition ($\lambda = 1.0$); transparent bars: no weight decay ($\lambda = 0$). Grokking models exhibit strong PC1 dominance (70–90%), while controls show diffuse spectra. This matches Figure 1 in Xu [2026b].

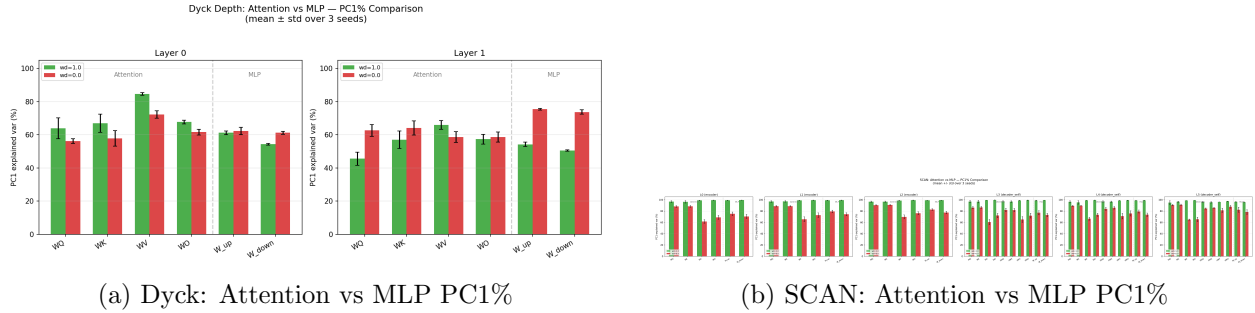


Figure 7: **Attention layers dominate spectral concentration.** PC1 explained variance decomposed by weight type. Attention projections (W_Q, W_K, W_V, W_O) show 70–85% concentration vs. 40–60% for MLP weights (W_{up}, W_{down}), indicating the grokking transition is primarily mediated by the attention mechanism. This is consistent with the attention-focused analysis of Xu [2026b].

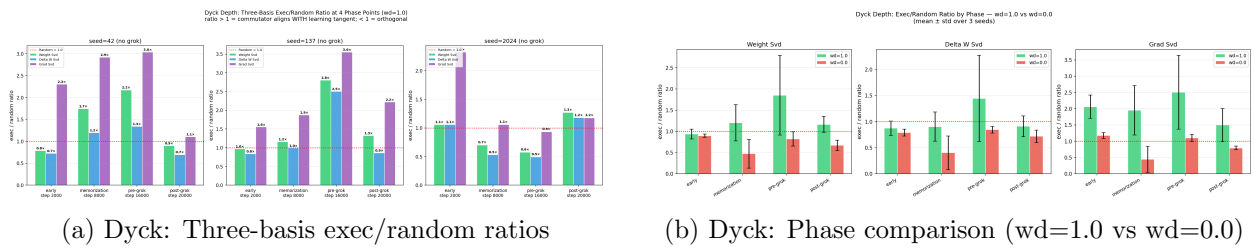


Figure 8: **Integrability breakdown at the pre-grok phase.** (a) Exec/random projection ratios for three bases (Weight SVD, ΔW SVD, Gradient SVD) across four training phases. Ratios spike to 2–3 \times at the pre-grok phase, indicating structured non-commutativity in the learning subspace. Compare with the exec/random ratio of 1.8–2.9 \times reported in Xu [2026b] for modular arithmetic. (b) No-weight-decay controls show no integrability breakdown.

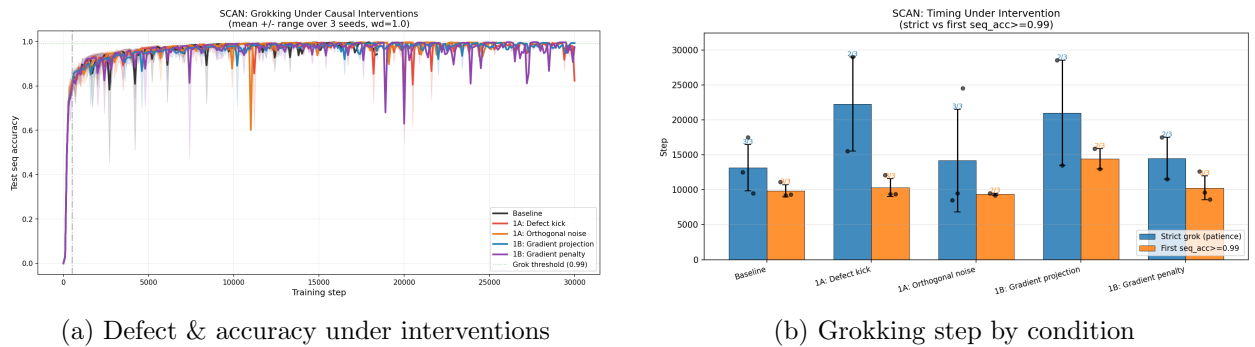


Figure 9: **SCAN: Causal interventions on the commutator defect.** (a) Defect (solid, log scale) and test accuracy (dashed) under five conditions. Mild boosting (1A-noise) accelerates grokking by $\sim 32\%$, but aggressive boosting (1A-kick) destabilizes the encoder–decoder dynamics and prevents grokking entirely. (b) Grokking step by condition. SCAN occupies an intermediate position between modular arithmetic (where boosting has no effect) and Dyck (where even aggressive boosting helps).

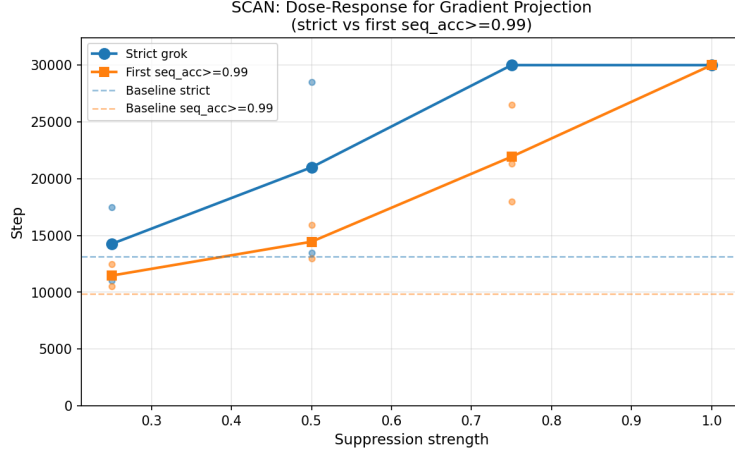


Figure 10: **SCAN: Dose–response relationship.** Grokking speed as a function of intervention strength. Suppression interventions show a monotonic dose–response, confirming graded causality. Compare with the Dyck dose–response (Figure 12) and Figure 14 in Xu [2026b] for modular arithmetic.

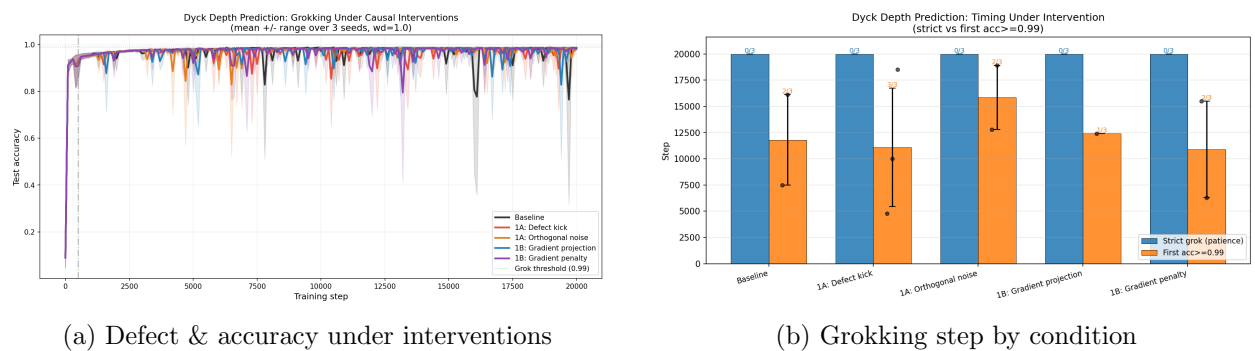


Figure 11: **Dyck: Causal interventions on the commutator defect.** (a) Defect (solid, log scale) and test accuracy (dashed) under five conditions. Both boosting interventions (1A-kick, 1A-noise) accelerate grokking; both suppression interventions (1B-project, 1B-penalty) delay it. Unlike SCAN, even aggressive boosting (1A-kick) accelerates rather than destabilizes. (b) Grokking step by condition. Dyck is the most responsive task: $\sim 50\%$ acceleration from 1A-kick, $\sim 50\%$ delay from 1B-project.

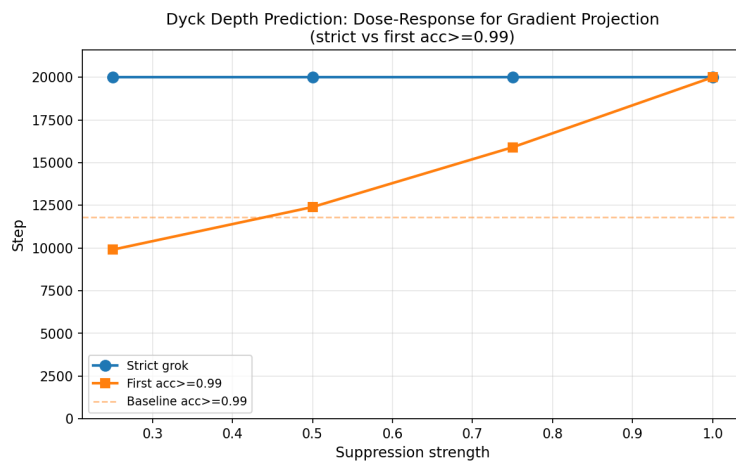


Figure 12: **Dyck: Dose-response relationship.** Grokking speed as a function of intervention strength. The monotonic relationship confirms graded causality for both boosting and suppression. Compare with the SCAN dose-response (Figure 10) and Figure 14 in Xu [2026b] for modular arithmetic.

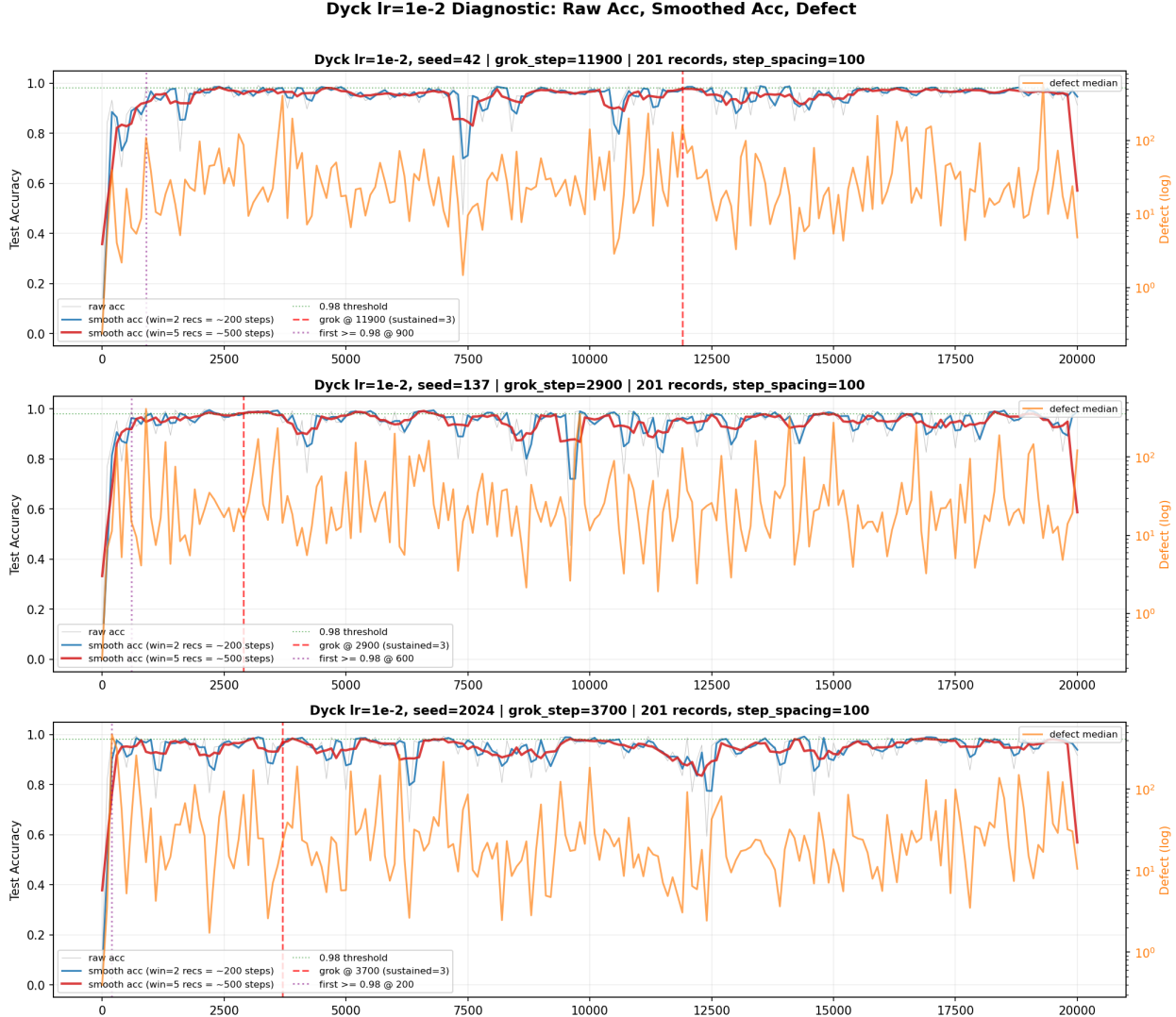


Figure 13: **Instability at $\eta = 10^{-2}$ on Dyck.** Raw test accuracy (gray), smoothed accuracy (blue: 200-step window; red: 500-step window), and commutator defect (orange, log scale) for all three seeds. The 0.98 threshold is shown in green. At this learning rate, accuracy oscillates violently (80+ threshold crossings). Seed 42 achieves sustained grokking only at step 11,900 despite first exceeding 0.98 at step 900. This instability regime was not observed in modular arithmetic [Xu, 2026b] and motivates the sustained-accuracy grokking criterion.

References

Barak, B., Edelman, B., Goel, S., Kakade, S., Malach, E., and Zhang, C. Hidden progress in deep learning: SGD learns parities near the computational limit. In *NeurIPS*, 2022.

Lake, B. M. and Baroni, M. Generalization without systematicity: On the compositional skills of sequence-to-sequence recurrent networks. In *ICML*, 2018.

Liu, Z., Michaud, E. J., and Tegmark, M. Omnigrok: Grokking beyond algorithmic data. In *ICLR*, 2023.

Liu, Z., Kitouni, O., Nolte, N., Michaud, E. J., Tegmark, M., and Williams, M. Towards understanding grokking: An effective theory of representation learning. In *NeurIPS*, 2023.

Loshchilov, I. and Hutter, F. Decoupled weight decay regularization. In *ICLR*, 2019.

Lyu, K., Jin, J., Li, Z., Du, S. S., Lee, J. D., and Hu, W. Dichotomy of early and late phase implicit biases can provably induce grokking. In *ICLR*, 2024.

Murty, S., Sharma, P., Andreas, J., and Manning, C. D. Grokking of hierarchical structure in vanilla transformers. In *ACL*, 2023.

Nanda, N., Chan, L., Lieberum, T., Smith, J., and Steinhardt, J. Progress measures for grokking via mechanistic interpretability. In *ICLR*, 2023.

Power, A., Burda, Y., Edwards, H., Babuschkin, I., and Misra, V. Grokking: Generalization beyond overfitting on small algorithmic datasets. In *MATH-AI Workshop, ICLR*, 2022.

Xu, Y. Low-dimensional execution manifolds in transformer learning dynamics: Evidence from modular arithmetic tasks. *arXiv preprint arXiv:2602.10496*, 2026.

Xu, Y. Low-dimensional and transversely curved optimization dynamics in grokking. *arXiv preprint*, 2026.

Yun, C., Bhojanapalli, S., Rawat, A. S., Reddi, S. J., and Kumar, S. Are transformers universal approximators of sequence-to-sequence functions? In *ICLR*, 2020.